Journal of Nuclear Materials 383 (2009) 237–243

Contents lists available at ScienceDirect

Journal of Nuclear Materials

journal homepage: www.elsevier.com/locate/jnucmat

Raman and XPS characterization of fuel–cladding interactions using miniature specimens

C.F. Windisch Jr. *, C.H. Henager Jr., M.H. Engelhard, W.D. Bennett

Pacific Northwest National Laboratory, Department of Fundamental and Computational Sciences, P.O. Box 999, Richland, WA 99352, United States

ARTICLE INFO

Article history:
Received 17 July 2008
Accepted 18 September 2008

ABSTRACT

A combination of laser Raman spectroscopy and X-ray photoelectron spectroscopy was applied in a study of fuel–cladding chemical interactions on miniature oxide-coated HT-9 disks at elevated temperature. The experiments were intended as a preliminary step toward the development of a quick-screening technique for candidate alloys for cladding materials and actinide-based mixed oxide fuel mixtures. The results indicated that laser Raman spectroscopy was capable of determining the major oxides on HT-9 and how they changed in composition due to heating. However, X-ray photoelectron spectroscopy was necessary to identify the role of the metallic phases and provide depth resolution. Using the two techniques the kinetics of chromia growth were shown to be affected by the presence of an applied oxide coating. A single replacement reaction involving residual reduced metal within the coating was also identified.

1. Introduction

Advanced recycle reactors (ARR) are being studied using a mixed oxide (MOX) fuel concept with an advanced tubular fuel cladding material, likely to be either HT-9 in a suitable heat treated condition or, possibly, a more current oxide dispersion hardened alloy based on a ferritic-martensitic alloy. The MOX fuel is likely to be a transuranic (TRU) mixture of the general form (U, Pu, Am, Np, Cm)-oxide containing the actinides Am, Np, and Cm in minor quantities yet to be determined, but perhaps up to 20% by volume, in order to facilitate burning of spent fuel products that are the source of the large quantities of radioactive burial waste present in the current once through fuel cycle. Since both the fuel mixture and cladding are still to be determined, their interactions under the operating conditions of a typical proposed ARR sodium-cooled reactor are unknown. Compounding the uncertainty, the conditions will be more severe than previous environments including temperatures above 723 K. The fuel–cladding chemical interactions (FCCI) are considered to be the life-limiting events of the fuel pin system and partly determine the level of burnup that can be tolerated. Cladding oxidation, corrosion, and embrittlement can lead to fuel pin rupture events that must be avoided. The recycled MOX fuel concept creates new uncertainties in our knowledge of cladding corrosion and lifetime calculations, not to mention the impact on fuel performance codes with associated uncertainties on fuel properties and swelling. These uncertainties must be addressed with a coordinated experimental and simulation campaign built around a limited number of actual fuel pins or rodlets tested in reactor. This paper addresses one such need, which is to be able to provide some initial screening data prior to initiating fuel pin or rodlet-type tests. This screening is especially relevant since there is a current lack of reactor test space for fuel pin testing.

Early tests in the Fast Flux Test Facility (FFTF) [US Department of Energy (DOE) Hanford Site, WA] with U-Pu driver fuel and HT-9 cladding and duct materials demonstrated the utility of the low swelling ferritic-martensitic steels as fuel cladding with operational fuel temperatures in the range of 873–933 K and up to 200 GWd $(MT)^{-1}$ burnup [1,2]. Although this is encouraging, there were fuel–cladding mechanical and chemical interactions observed with cesium, most notably causing cladding strain due to fuel swelling and mechanical contact [1]. Significant fuel–cladding chemical interactions (FCCI) are expected for the advanced fuel matrices proposed for the ARR. A literature review showed that the lanthanides-series fission products, in particular those observed by Pahl et al. [3], led to crack initiation and breaching of HT-9 cladding irradiated to 10 at.% (atomic percent) burnup in the Experimental Breeder Reactor II (EBR II) [US DOE Argonne National Laboratory, ID]. They saw numerous surface cracks in the breached inner cladding surface of HT-9 which were attributed to the following: (1) Formation of brittle bands in the inner cladding surface that was rich in the lanthanide-series (rare earths) fission products. Within the bands, iron and nickel had diffused out and deposited onto the fuel surface. Microhardness measurements showed the bands to be very hard at ambient conditions and contain numerous microcracks. (2) Soft layers of coarsened grains that lacked the lath structures of the tempered martensite. The layers were carbon depleted and penetrated by major cracks.

* Corresponding author. Tel.: +1 509 375 6538; fax: +1 509 375 2186.
E-mail address: cf.windisch@pnl.gov (C.F. Windisch Jr.).

0022-3115/$ - see front matter © 2008 Elsevier B.V. All rights reserved.
doi:10.1016/j.jnucmat.2008.09.028

The complexity of the FCCI by the lanthanide-series made it very difficult to predict the true nature of disruption in the HT-9 under the operating conditions when using known theoretical models [3]. Detailed post-irradiation data provided key information for understanding the processes leading to the observed HT-9 cladding failure. As has been observed by Tanaka et al. [4], even at moderate burnup of 47 GWd $(MT)^{-1}$, a cladding-fuel interaction layer can form as shown in Fig. 1 [4]. For MOX fuel, the fission yield is known to shift to non-oxidizable elements leaving excess oxygen available for cladding corrosion.

Knowledge of the chemical interactions of the fuel with the cladding is central to explaining the performance of advanced fuel types for the ARR. This paper focuses on developing a tool for prior screening of the phenomena. It is envisioned that such a technique could identify corrosion products as they form or evolve at elevated temperature and/or elucidate kinetic signatures that will support the theoretical modeling and mechanistic interpretation of the data. There is the potential for the US DOE Global Nuclear Energy Partnership (GNEP) to build on these experimental tools to hasten the advanced fuel qualification process. Mechanical properties testing of advanced cladding materials has suggested that ferritic-martensitic oxide dispersion strengthened (ODS) alloys are superior [5–10]. However, there is currently no data for the interactions of either HT-9 or developmental ODS alloys as cladding with the type of fuel envisioned for transuranic burning, which could contain a significant amount of Pu and the minor actinides (MA) of at least a few percent and perhaps much more [11–13]. The lack of data for these interactions highlights the need for a fast screening tool that places upper bounds on actinide concentrations while simultaneously identifying actinide elements and/or fission products that may enhance fuel cladding degradation.

Laser Raman spectroscopy (LRS) is a technique that can be applied in situ under realistic conditions to study corrosion at elevated temperatures and was the focus of this program to develop an accelerated screening approach for qualifying new fuels. In addition, we plan to use miniature 3-mm diameter disks of a suitable candidate alloy coated with oxides that serve as surrogate fuels and fuel-fission products as test specimens. The miniature specimens will be subjected to elevated temperatures and LRS spectra will be obtained in situ in an attempt to determine the changes in the composition of the oxides during heat treatment.

This paper reports on the results of initial studies that were performed ex situ (LRS data acquired at room temperature after heating in an open-air furnace and cooling the samples to room temperature) to analyze and follow the reactions between the fuel surrogate and the alloy as a function of heat treatment. The ex situ conditions gave spectra with excellent signal-to-noise and, consequently, were better able to assess the chemistry changes prior to performing the in situ measurements. Initial studies were performed on samples that were cleaned but not polished. The merits of using unpolished specimens can be debated, particularly in light of the LRS data, which suggested that oxide corrosion products were layered, and our decision to follow-up the LRS measurements with X-ray photoelectron spectroscopy (XPS) to help explain the LRS data. However, as reported below, the interface between the surrogate fuel and the alloy was remarkably sharp for these samples despite the lack of polishing of the original uncoated alloy. As a result, it proved to be a suitable reference point for observing and interpreting the compositional changes that occurred across it due to heat treatment. Additional studies are underway using polished samples and a wider variety of surrogate fuel materials that will add to the breadth and precision of the measurements reported here. In situ measurements are also being performed using a Raman microprobe coupled with a high-temperature microscope stage.

2. Experimental procedure

Miniature, 3-mm diameter, HT-9 samples were "punched" from a 0.2-mm thick sheet of material obtained from FFTF Core Demonstration heats. Composition was reported by the manufacturer in Table 1 with balance being Fe.

Some samples were tested without any coating. Others were first coated with a thin film of yttria-stabilized zirconia (YSZ) deposited by DC reactive magnetron sputtering in a 71-cm box coater. The sputtering source was a 7.6-cm diameter Mighty Mak™ cathode (US, Inc.) and the chamber was configured for single planetary rotation of the substrates above the cathode. Substrates were cleaned prior to film deposition using a Commonwealth Mark II ion source and then the sputtered coatings were applied at a chamber pressure of 0.8 Pa. The starting target material for this work was a Y/Zr (85/15) alloy. All deposits were made using a mixture of Ar + 5% O_2. The targets were cleaned in 100% Ar for 600 s prior to gradually increasing the O_2. A 1.5 kW power supply (Advanced Energy model MDX 1.5 K) running at 0.6 DC amp was used for both depositions. A custom substrate holder was fabricated for use with the 3-mm diameter substrates.

Some of the uncoated and coated samples were heated at 973 K for various times using an open-air electric furnace. Prior to heating, the samples were degreased using acetone but without additional surface preparation, e.g. grinding or polishing. Once heated, the samples were cooled to room temperature and analyzed with LRS and XPS.

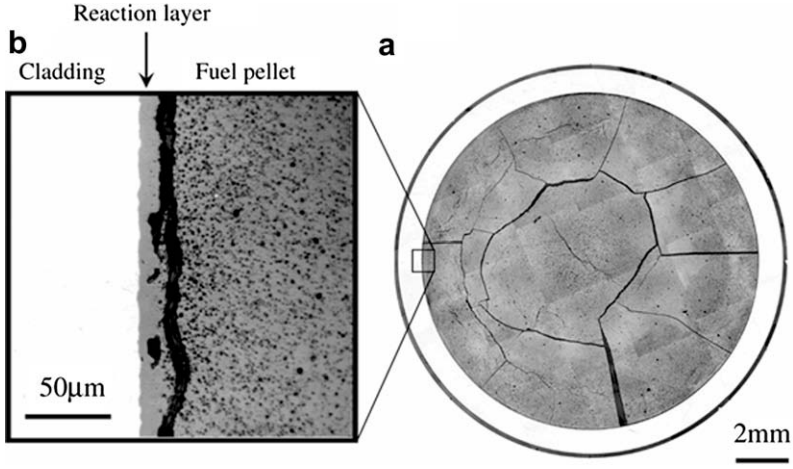

Fig. 1. FCCI between UO_2–PuO_2 (2.6%) fuel and Zircaloy-2 cladding following a burnup of 47 GWd $(MT)^{-1}$ with a clearly defined cladding-fuel interaction layer [4].

Table 1
HT-9 Composition.

Material	Cr	C	Si	Mn	W	V	Mo	Ni
HT-9	11.8	0.21	0.29	0.53	0.52	0.33	1.06	0.6

Raman spectra were acquired using a Spex (Edison, NJ) Model 1877 spectrometer equipped with a Princeton Instruments (Trenton, NJ) liquid nitrogen cooled charge-coupled detector (LN/CCD). The 488.0-nm line of a Coherent (Santa Clara, CA) Innova 307 Ar^+ ion laser was used for excitation and sample collection was in the backscattering configuration. The slit width was 400 μm and the exposure time was 1000 s for all samples. Spectral analysis was performed using Galactic Industries (Salem, NH) Grams/32AI software. The estimated uncertainty of the peak frequencies was ±1 cm^{-1}.

XPS measurements were performed using a Physical Electronics (Chanhassen, MN) Quantum 2000 Scanning ESCA Microprobe. This system used a focused monochromatic Al Kα X-ray (1486.7 eV) source and a spherical section analyzer. The instrument was equipped with a 16 element multichannel detector. The X-ray beam, 40 W and 200 μm in diameter, was incident normal to the sample while the photoelectron detector was at 45° off-normal. The high energy resolution photoemission spectrum was collected using a pass energy of 46.95 eV. For the $Ag3d_{5/2}$ line, these conditions produced a frequency width at half-maximum (FWHM) of better than 0.98 eV. The binding energy (BE) scale is calibrated using the $Cu2p_{3/2}$ feature at 932.62 ± 0.05 eV and Au4f at 83.96 ± 0.05 eV for known standards. The sample experienced variable degrees of charging. Low energy electrons, at ~1 eV and 20 μA, and low energy Ar^+ ions were used to minimize this charging.

The HT-9 samples were mechanically mounted onto a XPS sample holder using stainless steal screws and molybdenum mask. The XPS sample holder was placed into the XPS vacuum introduction system and pumped to $<1 \times 10^{-4}$ Pa using a turbo-molecular pumping system prior to moving into the main spectrometer ultra high vacuum system. The spectrometer vacuum system pressure was maintained at $<7 \times 10^{-7}$ Pa during analysis and pumped using a series of sputter ion pumps.

Sample sputtering was performed using 2 kV Ar^+ ions rastered over a 2 mm × 2 mm area of the specimen. The ion gun incident angle was 45°. The sputter rate for these ion gun conditions was calibrated at a rate of 0.13 nm s^{-1}, using known SiO_2 reference material. The vacuum chamber pressure during analysis was $<1.3 \times 10^{-6}$ Pa. During a sputter depth profile study, XPS spectra were collected after arbitrary sputtering time increments (cycles). Sputter depth can therefore be expressed in terms of the number of sputtering cycles or time of sputtering or, by using the SiO_2 reference, estimated in geometric units.

3. Results and discussion

3.1. Uncoated HT-9

As shown in Fig. 2, the Raman spectrum of an as-received HT-9 sample (marked 0.0 ks) exhibited a strong peak at approximately 685 cm^{-1} that is attributed to the spinel oxide Fe_2CrO_4. The similar spinel $FeCr_2O_4$ was reported to have a strong Raman band at this frequency [14]. Since all of the compositionally different spinels in the Fe–Ni–Cr oxide family have Raman spectra that are similar with a major peak assigned to the symmetric stretch of the group of octahedrally oriented oxygen ions, whose frequency ranges between roughly 660 cm^{-1} and 700 cm^{-1}, the revised assignment for our data is reasonable and also more consistent with the XPS results reported below. Small features at lower frequencies indicate the presence of other components, especially some Cr_2O_3 (chromia), which is identified by the peak at 549 cm^{-1} [15]. In addition to the spinel oxide, another major component was carbon, which gave rise to a strong broad band at 1348 cm^{-1} (not shown). Significant carbon was also identified on these samples using XPS.

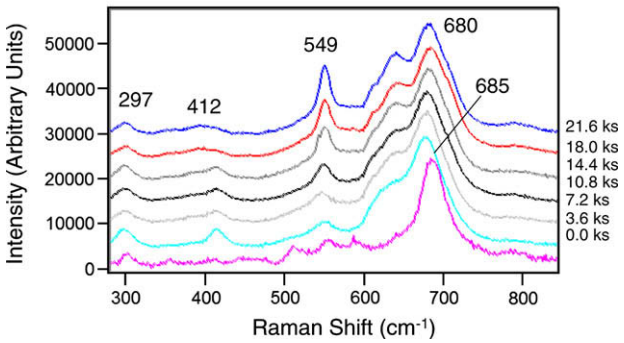

Fig. 2. Raman spectra of corrosion products on HT-9 sample without YSZ coating as a function of time of heating at 973 K in air.

When samples of the HT-9 were heated at 973 K in air for varying times up to 21.6 ks, their Raman spectra (acquired ex situ in air at room temperature) showed significant changes, both in signal intensities and in the number and frequencies of the peaks. These changes are shown in Fig. 2. The most significant changes were an increase in the total Raman intensities across the spectrum (not shown explicitly in Fig. 2 because the spectra were all normalized in intensity relative to the spinel band), which indicates an increase in film thickness (increased corrosion products) with time at temperature. In addition, the intensity of the Cr_2O_3 peak at 549 cm^{-1} increased relative to that of the spinel peak. The spinel peak was also observed to shift slightly to lower frequency (680 cm^{-1}) and to broaden, with a low-frequency shoulder becoming relatively intense and well-resolved at 21.6 ks. The shoulder can be attributed, at least partly, to another band from Cr_2O_3 previously reported to occur at 617 cm^{-1} [15]. Variation in spinel composition and structure (for example, replacing Ni^{2+} for Fe^{2+} or Fe^{3+} for Cr^{+3} in the oxide) is also known to have an influence on the spinel band. It is possible that some Fe_3O_4 (magnetite) was present in the oxide, based on the XPS results reported below and the assignment of a strong band at 663 cm^{-1} to this oxide as reported in the literature [15]. Another observation is that a set of bands at lower frequency, including 297 cm^{-1} and 412 cm^{-1}, which are weak in the original spectrum, grow in at intermediate times (between 3.6 and 14.4 ks) and then appear to diminish. These bands are assigned to α-Fe_2O_3 (hematite) [14,15].

XPS measurements on the as-received sample indicate the presence of a relatively thick oxide film (approximately 800 nm if taken as the distance from the surface to the depth where the oxygen concentration had diminished to 50% of its surface concentration) that formed during and/or following fabrication. The composition near the surface is approximately 2:1 (atomic concentration of Fe:Cr). This is consistent with the Raman spectra indicating the presence of a spinel, most likely Fe_2CrO_4. Other iron oxides may also be present at smaller concentrations, including α-Fe_2O_3, FeO and/or Fe_3O_4. The latter two would give Raman bands that would be either weak (in the case of FeO) or obscured (by the iron–chromium spinel) in the Raman spectra. As previously noted, significant carbon was also identified on the sample by XPS prior to any heating in air.

The XPS spectrum of a sample of HT-9 heated in air for 21.6 ks showed significant changes, consistent with the Raman spectra. A very thick, approximately 1.25 μm, film was measured and its

major component was chromium with increasing amounts of iron deeper within the film. This supports changes in Cr_2O_3 and spinel composition similar to the Raman spectra, although the distribution of these oxides within the film is somewhat ambiguous due to the appreciable thickness of the film and the gradual variations of compositions with depth within it. The latter may also be partly attributed to unevenness in the interfaces.

3.2. Coated HT-9

As shown in Fig. 3, the Raman spectrum of an HT-9 sample that was coated with YSZ but prior to heat treatment (labeled 0.0 ks) was similar to that of the uncoated sample prior to heat treatment (Fig. 2 and 0.0 ks). The result indicates that the thin YSZ film was insufficient to contribute peaks to the Raman spectrum. On the other hand, XPS depth profiling was able to clearly demonstrate the presence, as well as resolve the thickness, of the YSZ layer as shown in the depth profile of the non-heated sample in Fig. 4. A sputter time of about 1.8 ks was sufficient to remove the YSZ layer. Based on the sputter rate of SiO_2 (0.13 nm s^{-1}), this corresponded to a film thickness of about 230 nm. The XPS spectra also showed that the film deposition conditions removed most of the carbon contaminant observed in the spectrum of the uncoated sample.

The XPS depth profile in Fig. 4 also indicates a (sublayer) oxide remained under the YSZ film that contained both iron and chromium similar in their concentration relationship (Fe > Cr) to that of the uncoated specimen. This is consistent with the similarity between the Raman spectra of the oxides on the coated and uncoated samples prior to heat treatment (spectra labeled 0.0 ks in Figs. 2 and 3). As shown in Fig. 4, some Zr can also be seen to extend into the sublayer oxide.

It is important to note that the Zr signal in the depth profile in Fig. 4 is quite "flat" over the 230 nm region near the surface and that the initial drop in Zr signal is quite sharp, falling to about half its value within 30 nm. Only a much smaller amount of Zr appears to penetrate deeper. The abruptness of this drop speaks to a relatively sharp interface at the YSZ-sublayer interface. While not ruling out the role of roughness of the original uncoated alloy surface (on subsequent coating and heating steps), the result indicates that the starting point shown in Fig. 4 (i.e. composition before heat treatment) has suitable "resolution" to interpret changes due to heat treatment in terms of compositional variations across the YSZ-sublayer oxide interface.

Close scrutiny of the Zr peaks in the XPS spectra reveals that the YSZ layer also contained small amounts of reduced Zr metal (Fig. 5). A $Zr3d_{5/2}$ peak at lower binding energy (approximately 180.3 eV) is clearly present in the spectra obtained from the near surface layers of the film during sputter depth profiling. This peak is indicative of Zr valence <+4. The $Zr3d_{5/2}$ peak for zero-valent Zr is reported at ca. 178.9 eV, compared to ZrO_2 (182.2 eV). The presence of this reduced Zr is proposed to be important in the oxidation behavior of the material as reported below.

As shown in Fig. 3, heat treatment at 973 K in air resulted in the YSZ-coated samples oxidizing to some extent but differently than uncoated samples reported previously. First, the amount of additional Cr_2O_3 formed (indicated by the peak at 549 cm^{-1}) was very little, if any, over the course of 21.6 ks (6 h). Even after 86.4 ks (one day) at temperature, the amount of Cr_2O_3 was only slightly more that in the original film. In contrast, there is a large increase in the bands at 297 and 412 cm^{-1}, assigned to α-Fe_2O_3, during the first 3.6 ks. Between 21.6 ks and 86.4 ks, the α-Fe_2O_3 diminished significantly. There is a significant change in the bandwidth and structure of the spinel peak, broadening to lower frequency and exhibiting a well defined maximum at intermediate times (14.4 ks), then becoming broader and somewhat obscure at longer times.

An explanation for the Raman spectra of the coated films is apparent from the results of the XPS measurements on a coated HT-9 sample that was heated for 21.6 ks. As shown in Fig. 6, the YSZ layer remains intact but it now shows a small but significant increase in the amount of Fe (as well as a small amount of Cr) compared to the composition before heating (Fig. 4). This is also

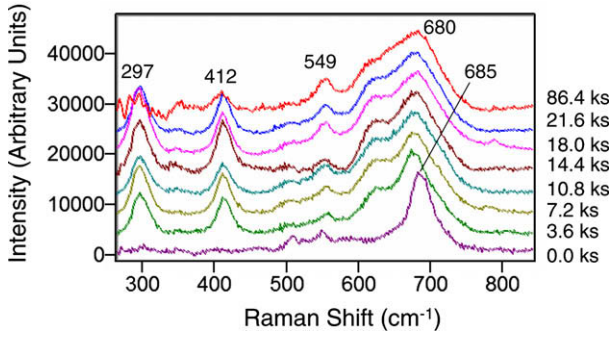

Fig. 3. Raman spectra of corrosion products on HT-9 sample with ~230-nm thick YSZ coating as a function of time of heating at 973 K in air.

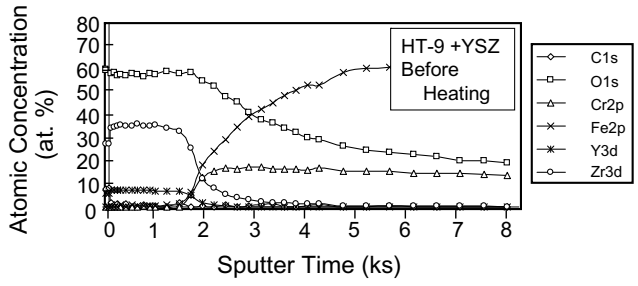

Fig. 4. XPS depth profile of HT-9 sample with YSZ coating before heating at 973 K in air.

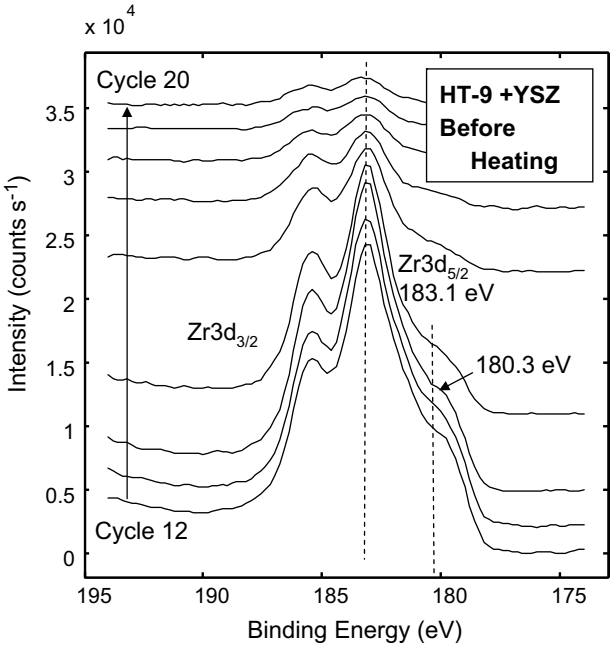

Fig. 5. Variation of XPS $Zr3d_{5/2}$ peaks with sputter depth for HT-9 sample with YSZ coating, before heating at 973 K in air. The peak at 180.3 eV is attributed to a reduced form of Zr.

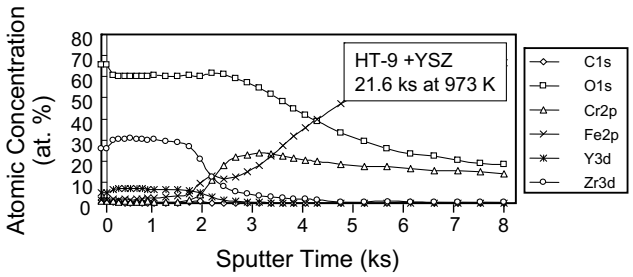

Fig. 6. XPS depth profile of HT-9 sample with YSZ coating, after heating in air at 973 K for 21.6 ks.

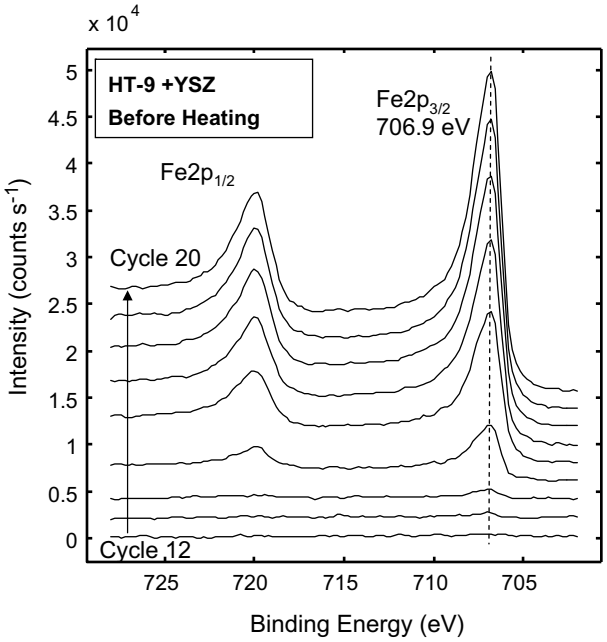

Fig. 7. Variation of XPS $Fe2p_{3/2}$ peaks with sputter depth for HT-9 sample with YSZ coating, before heating at 973 K in air.

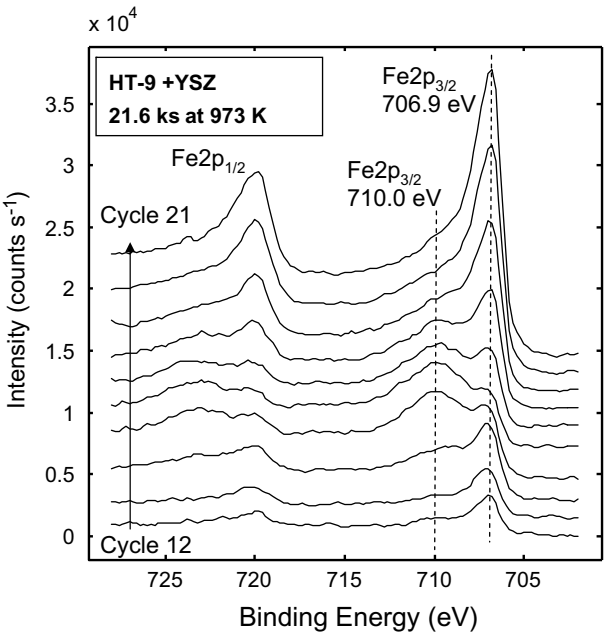

Fig. 8. Variation of XPS $Fe2p_{3/2}$ peaks with sputter depth for HT-9 sample with YSZ coating, after heating at 973 K in air for 21.6 ks.

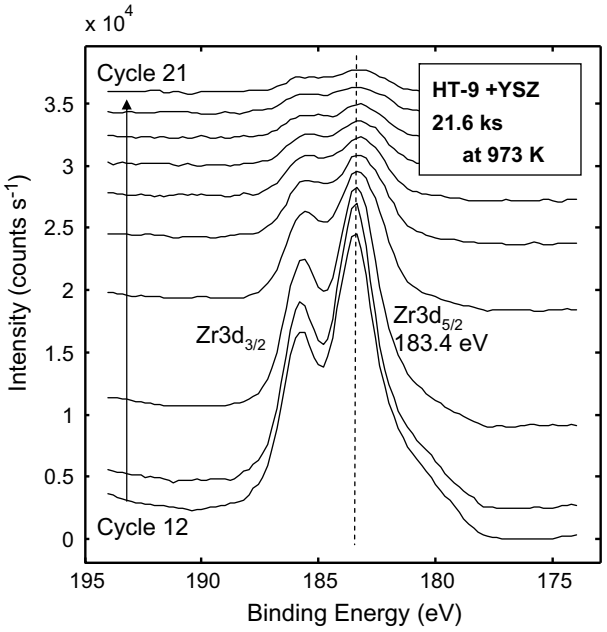

Fig. 9. Variation of XPS $Zr3d_{5/2}$ peaks with sputter depth for HT-9 sample with YSZ coating, after heating at 973 K in air for 21.6 ks.

illustrated in the XPS depth profiles of the Fe2p region in Figs. 7 and 8. Before heating, the Fe is essentially absent in the spectra obtained during cycles 12–14 where the amount of ZrO_2 is significant (Fig. 6). However, as shown in Fig. 8, after heat treatment, there is a significant increase in the amount of Fe, both oxidized (710.0 eV) and reduced (706.9 eV), at similar depths. The binding energy for the $Fe2p_{3/2}$ peak from zero valent Fe is 707.0 eV [16]. The likely reaction or reaction step that results in the reduced Fe is a single replacement-type involving reduced Zr and an iron oxide. The XPS depth profile of the $Zr3d_{5/2}$ region confirms this. As shown in Fig. 9, the lower binding energy shoulder (180.3 eV) originally assigned to reduced Zr (Fig. 5) is significantly diminished after the sample is subjected to heat treatment.

Along with the oxidation–reduction reaction involving reduced Zr and an iron oxide, other changes in composition of the corrosion film with heat treatment need to be noted. As shown in Fig. 8, at slightly larger depths (cycles 15-19), an $Fe2p_{3/2}$ peak at higher binding energy grows in and this peak is attributed to Fe_2O_3 (710.9 eV) [16]. The presence of Fe_2O_3 is consistent with the Raman spectra reported above (Fig. 3) that indicated α-Fe_2O_3. Another observation from both the Raman spectra and the XPS depth profiles is that the composition of the spinel under the YSZ film appears to change with time during heat treatment, transitioning from an iron-rich Fe_2CrO_4 composition to a chromium-rich $FeCr_2O_4$ composition. The Raman showed this by a marked change in the bandwidth of the spinel peak (indicating a mixed composition) and a shift to lower frequencies (consistent with increased concentrations of the heavier Cr atoms). The XPS spectra clearly indicate a difference in the Fe:Cr atomic ratio in the oxide film under the YSZ for the coated HT-9 samples before and after heat treatment. Before heat treatment the ratio is significantly greater than unity consistent with Fe_2CrO_4 (Fig. 4), while after heat treatment the ratio is less that unity just under the YSZ film consistent with $FeCr_2O_4$ (Fig. 6).

3.3. Proposed reaction

In summary, the above results indicate that the YSZ coatings that were deposited on the HT-9 samples contained significant amounts of reduced Zr and that this Zr reacted with the metal oxide films under the YSZ during early times at temperature. The reaction produced significant amounts of reduce Fe and (to a lesser extent) Cr (spectra not shown) in the film during this time. A possible net reaction consistent with the oxidation of metallic Zn, the formation of both metallic Fe and α-Fe_2O_3, and the variations in spinel composition suggested by changes in the Raman bands associated with the spinel is the following:

$$4Fe_2CrO_4 + Zr \rightarrow 2Fe + 2\alpha\text{-}Fe_2O_3 + 2FeCr_2O_4 + ZrO_2 \quad (1)$$

The mechanism for this reaction is predictably complicated and probably involves dissociation of Fe_2CrO_4 in the corrosion products under-layer and transport of the resulting ions, presumably mostly Fe^{3+} and O^{2-}, across the boundary with the YSZ, followed by reduction of Fe^{3+} (as described above) by the residual Zr within the YSZ. The chromate species and oxide ions respond by transport and deposition/reaction steps of their own, resulting in the observed and varied layered structure that persists at the 21.6-ks exposure mark.

3.4. Implications on oxygen transport

The above results include the observation that significant amounts of reduced metal, whether Zr (initially) or Fe (later) remain in the film even after exposure for up to 21.6 ks at 973 K. For this to happen, the transport of oxygen from outside of the YSZ to subsurface metal and metal oxides has to be impeded. Clearly, the YSZ layer acts as a barrier to oxygen transport during this time, even though several redox reactions, along with diffusion of ionic and/or possibly other molecular species, occurred within the layer itself. The role of the YSZ layer on the oxidation kinetics of the HT-9 is illustrated in Fig. 10. The Raman intensity ratio of the 549 cm^{-1} band (Cr_2O_3) to the 680 cm^{-1} band (spinel) increases at a substantially higher rate in the absence of the film. Over 21.6-ks (6-h) exposure at 973 K, very little Cr_2O_3 forms in the presence of the film. If the chromia formation is an indication of the extent of the HT-9 corrosion, the presence of the YSZ film clearly slows down this corrosion. The result is consistent with previous studies on zirconium oxides as components of high-temperature anti-corrosion coatings [17,18]. Interestingly, at longer exposure times, the inhibitory role of YSZ may be diminished. As shown in the Raman spectrum of a YSZ-coated sample after 86.4-ks (1-day) exposure to 973 K in air (Fig. 3), the α-Fe_2O_3, which formed during the early-time reactions involving reduced Zr and the iron oxides, has significantly decreased (peaks at 297 cm^{-1} and 412 cm^{-1} are weaker) and a small additional amount of Cr_2O_3 has appeared to form (slightly stronger peak at 549 cm^{-1}). This suggests additional chemical reactions occur at longer times, possibly including reincorporation of the Fe (from Fe_2O_3) into the spinel and oxidation of additional Cr from the base metal. If the latter occurs, then oxygen diffusing from outside of the YSZ layer is a possibility, suggesting the efficacy of the film as a corrosion inhibitor decreases over longer times at temperature.

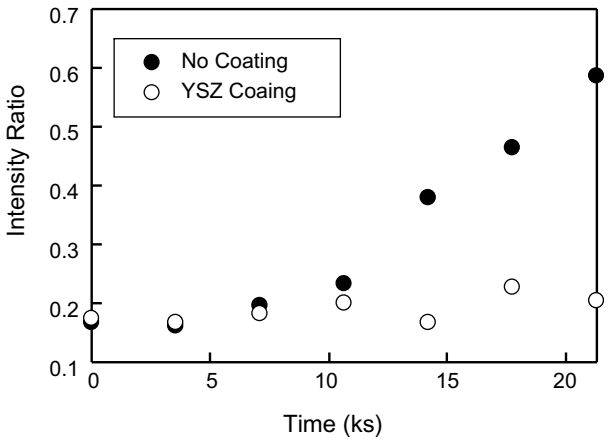

Fig. 10. Variation of the intensity ratio (C/S) for the Raman peaks due to chromia (C) and spinel (S) in the corrosion film on HT-9 as a function of time of heating at 973 K in air. The influence of the YSZ coating on changes in composition of the film is clearly evident.

4. Conclusions

A combination of LRS and XPS was used to study changes in the oxide on HT-9 as well as the interface between HT-9 and a coating of yttria-stabilized zirconia (surrogate fuel) in miniature specimens at 973 K. The LRS data revealed the composition of the major reactant and product oxide phases and, with the help of XPS to discriminate metallic phases as well as depth resolution, it was possible to identify reactions that occurred within the oxide layers. The principal reaction products on uncoated samples were found to be iron chromium spinel oxides (Fe_2CrO_4 and $FeCr_2O_4$), α-Fe_2O_3, and Cr_2O_3, with the latter oxide increasing in proportion to the spinel with time of heating. Coated samples showed some similarities but the kinetics of Cr_2O_3 growth were much slower when the film was present. In addition, significantly more α-Fe_2O_3 formed on the coated samples and, with the help of XPS analysis, this was attributed to a single replacement reaction involving the oxidation of residual reduced Zr within the as-formed film. Given the sensitivity of LRS to the major oxides involved in the simulated fuel–cladding interactions, the results lend promise to the use of LRS and a screening tool for the developing new fuels and cladding materials. Future work will include adapting the approach for in situ studies and building a more complete data base of combined LRS–XPS results. It is hoped that an unambiguous relationship between data from the two techniques can be established so that LRS can be used independently as part of an in situ screening procedure for candidate materials.

Acknowledgements

This research was sponsored by the Sustainable Nuclear Power Initiative at the Pacific Northwest National Laboratory (PNNL) under the Laboratory Directed Research and Development program. PNNL is operated by Battelle Memorial Institute for the US Department of Energy under Contract No. DE-AC06-76RLO1830. A portion of the research was performed in the Environmental Molecular Sciences Laboratory, a national scientific user facility sponsored by the Department of Energy's Office of Biological and Environmental Research and located at PNNL.

References

[1] D.C. Crawford, D.L. Porter, S.L. Hayes, J. Nucl. Mater. 371 (2007) 202.
[2] A.E. Bridges, A.E. Waltar, R.D. Leggett, R.B. Baker, J.L. Ethridge, Nucl. Technol. 102 (1993) 353.
[3] R.G. Pahl, C.E. Lahm, S.L. Hayes, J. Nucl. Mater. 204 (1993) 141.
[4] K. Tanaka, K. Maeda, S. Sasaki, Y. Ikusawa, T. Abe, J. Nucl. Mater. 357 (2006) 58.
[5] T. Narita, S. Ukai, T. Kaito, S. Ohtsuka, Y. Matsuda, J. Nucl. Sci. Technol. 45 (2008) 99.
[6] S. Ukai, S. Ohtsuka, J. Nucl. Mater. 367–370 (2007) 234.
[7] S. Ukai, T. Kaito, S. Ohtsuka, T. Narita, H. Sakasegawa, Trans. Am. Nucl. Soc. 94 (2006) 786.
[8] S. Ukai, T. Kaito, M. Seki, A.A. Mayorshin, O.V. Shishalov, J. Nucl. Sci. Technol. 42 (2005) 109.

[9] S. Ukai, T. Kaito, S. Ohtsuka, T. Narita, M. Fujiwara, T. Kobayashi, ISIJ Int. 43 (2003) 2038.
[10] S. Ukai, M. Fujiwara, J. Nucl. Mater. 307–311 (2002) 749.
[11] D. Warin, J. Nucl. Sci. Technol. 44 (2007) 410.
[12] L.F. Miller, J. Preston, T. Anderson, J. McComm, F.R. Mynatt, L. Van Den Durpel, Trans. Am. Nucl. Soc. 95 (2006) 222.
[13] W.J. Carmack, D.J. Utterbeck, Trans. Am. Nucl. Soc. 93 (2005) 747.
[14] S.C. Tjong, Mater. Res. Bull. 18 (1983) 157.
[15] D.J. Gardiner, C.J. Littleton, K.M. Thomas, K.N. Strafford, Oxid. Met. 27 (1987) 57.
[16] J.F. Moulder, W.F. Stickle, P.E. Sobol, K.D. Bomben, Handbook of X-Ray Photoelectron Spectroscopy, Physical Electronics, Inc., Eden Prairie, MN, 1995.
[17] M. Atik, J. Zarzycki, C. R'Kha, J. Mater. Sci. Lett. 13 (1994) 266.
[18] K. Kitke, W. Osterle, A. Skopp, M. Woydt, J. Raman Spectrosc. 32 (2001) 1008.